

Article

Novel BODIPY Conjugates with Myrtenol: Design, Spectral Characteristics, and Possibilities for Practical Application

Galina B. Guseva ¹, Elena V. Antina ¹, Mikhail B. Berezin ¹, Liliya E. Nikitina ^{2,3}, Ilmir R. Gilfanov ^{3,4}, Roman S. Pavelyev ³, Svetlana A. Lisovskaya ^{2,3,5}, Larisa L. Frolova ⁶, Olga V. Ostolopovskaya ^{2,3}, Ilfat Z. Rakhmatullin ⁷, Vladimir V. Klochkov ⁷, Elena Y. Trizna ³ and Airat R. Kayumov ^{3,*}

- ¹ G.A. Krestov Institute of Solution Chemistry of the Russian Academy of Sciences, 153045 Ivanovo, Russia; gbg@isc-ras.ru (G.B.G.); eva@isc-ras.ru (E.V.A.); mbb@isc-ras.ru (M.B.B.)
- ² Faculty of Medicine and Biology, Kazan State Medical University, 420012 Kazan, Russia; nikitl@mail.ru (L.E.N.); s_lisovskaya@mail.ru (S.A.L.); olga-ov.kirill@mail.ru (O.V.O.)
- ³ Institute of Fundamental Medicine and Biology, Kazan Federal University, 420008 Kazan, Russia; ilmir.gilfanov@gmail.com (I.R.G.); rpavelyev@gmail.com (R.S.P.); trizna91@mail.ru (E.Y.T.)
- ⁴ Institute of Petroleum, Chemistry and Nanotechnologies, Kazan National Research Technological University, 420015 Kazan, Russia
- ⁵ Scientific Research Institute of Epidemiology and Microbiology, 420015 Kazan, Russia
- ⁶ Institute of Chemistry, Federal Research Center “Komi Scientific Centre”, Ural Branch, Russian Academy of Sciences, 167000 Syktyvkar, Russia; frolova-ll@chemi.komisc.ru
- ⁷ Institute of Physics, Kazan Federal University, 420008 Kazan, Russia; ilfat89rakhmatullin@gmail.com (I.Z.R.); klochkov@gmail.com (V.V.K.)
- * Correspondence: kairatr@yandex.ru



Citation: Guseva, G.B.; Antina, E.V.; Berezin, M.B.; Nikitina, L.E.; Gilfanov, I.R.; Pavelyev, R.S.; Lisovskaya, S.A.; Frolova, L.L.; Ostolopovskaya, O.V.; Rakhmatullin, I.Z.; et al. Novel BODIPY Conjugates with Myrtenol: Design, Spectral Characteristics, and Possibilities for Practical Application. *Inorganics* **2023**, *11*, 241. <https://doi.org/10.3390/inorganics11060241>

Academic Editors: Vladimir Arion, Marvin Antonio Soriano-Ursúa and Bhaskar C. Das

Received: 21 April 2023

Revised: 19 May 2023

Accepted: 31 May 2023

Published: 3 June 2023



Copyright: © 2023 by the authors. Licensee MDPI, Basel, Switzerland. This article is an open access article distributed under the terms and conditions of the Creative Commons Attribution (CC BY) license (<https://creativecommons.org/licenses/by/4.0/>).

Abstract: The synthesis of new fluorescent probes, based on biocompatible luminophors and exhibiting various specificities, is intensively developed worldwide. Many luminophors contain a hydrophobic group that limits their application for cell staining under vital conditions. Herein, we report the synthesis of two BODIPY molecules—*BF*₂-*meso*-(4-butan/pentanamido-*N*-(((1*S*,5*R*)-6,6-dimethylbicyclo [3.1.1]hept-2-en-2-yl)methyl)-*N,N*-dimethylpropan-1-aminium)-3,3',5,5'-tetramethyl-2,2'-dipyrrromethene bromides—designed as **10**, **11** with a spacer of either four or three CH₂ groups in length, respectively. These molecules present conjugates of BODIPY luminophors with (+)-myrtenol via a quaternary ammonium group. Both terpene-BODIPY conjugates demonstrated high fluorescence efficiency in various solvents such as OctOH, DMSO and water, and were characterized by their stability at pH 1.65–9.18. The fusion of the myrtenol, a monocyclic terpene, to the BODIPY fluorophore in the *meso*-substituent facilitated their penetration into the filamentous fungi *Fusarium solani*, while impairing the binding of the latter with *S. aureus*, *K. pneumoniae* and *P. aeruginosa*. The additional quaternary ammonium group between the myrtenol and fluorophore moieties restored the bacterial cell-staining while it did not affect the staining of fungi. Finally, the BODIPY conjugate **11** was able to stain both Gram-positive and Gram-negative bacteria by its interaction with their cell wall (or the membrane), as well as penetrating into filamentous fungi *F. solani* and staining their mitochondria.

Keywords: BODIPY conjugates; (+)-myrtenol; spectral properties; biovisualization

1. Introduction

Fluorescent dyes absorbing and emitting in the visible and near-IR regions are promising for the development of fluorescent probes for the labeling and visualization of cells, their organelles and compartments. The dyes absorbing and emitting in the long-wavelength spectra are characterized by a higher efficiency of signal recording due to the higher permeability of the cell [1–5]. Compared to other fluorescent dyes, BODIPY are attractive for practical applications due to their excellent photophysical properties—narrow absorption and emission spectra, intense fluorescence and simple signal modulation [6,7]. In our recent

works [8,9] biomarkers **1**, **2**, based on the BODIPYs with an ester group $-(\text{CH}_2)_n\text{COOCH}_3$, $n = 3$ or 4 in dipyrromethene *meso*-spacer, were described (Figure 1).

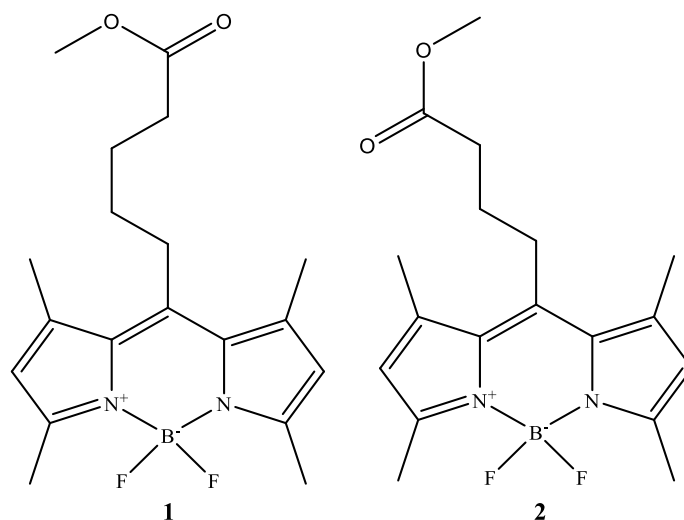


Figure 1. Structural representation of the BODIPYs **1**, **2**.

The *meso*-substituted BODIPYs **1**, **2** (Figure 1) preferentially stain Gram-positive bacteria and can be proposed for the differential staining of Gram-positive and Gram-negative bacteria in mixed cultures [8]. These luminophores accumulate in the cytoplasm of mammalian cells, and giving a polar micro-speckled staining pattern which is more intensive in tumor cells when compared to normal fibroblasts [8,9]. Moreover, BODIPYs have been proposed as a fluorescent marker when assessing the features and structural changes of cellular membranes of mammalian and fungal cells [9].

One of the promising BODIPY applications in the field of conjugation with biomolecules is devoted to the labeling of vitamins, hormones, lipids and other biomolecules to control the processes of their transport, localization in target cells and metabolism [10–13]. Being fused with various biomolecules, BODIPY could act as a biomarker of therapeutic agents and solve several tasks, such as depicting the cellular localization of the latter and real-time imaging the suppression of pathogenic microflora and cancer cells, thus providing huge potential for the practical application of BODIPY conjugates in medicine [1].

Recently, we have reported spectral and biological properties of the BODIPY **1** and its conjugate with (+)-myrtenol **3** (BODIPY **4**), see Figure 2 [14]. (+)-Myrtenol **3** is a bicyclic monoterpene alcohol found in the essential oils of various plants, whose crude extracts show anti-inflammatory, antinociceptive and antifungal activities, have a pleasant odor, and are widely used in cosmetics [15–20]. Moreover, our findings confirmed that (+)-myrtenol is capable of increasing the efficiency of various antimicrobial, antifungal, and antiseptic drugs, exhibiting a pronounced synergy with these compounds [21].

The conjugate **4** exhibits a high quantum yield (to ~100%) in the region of 515–518 nm and effectively penetrates the membranes of both bacterial and fungal cells and, therefore, can be used to examine the features of a broad spectrum of Gram-positive and Gram-negative bacteria, and pathogenic fungi as well [14]. Moreover, BODIPY **4** exhibited a moderate tropism to the subcellular structures in mammalian cells (e.g., mitochondria), thereby providing an attractive scaffold for fluorophores to examine these particular organelles.

BODIPYs **1,2** were used as initial compounds to create conjugates **10**, **11** carrying a quaternary ammonium fragments in addition to (+)-myrtenol. The quaternary ammonium compounds, in particular benzyldimethyl[3-(myristoylamino)propyl]ammonium chloride monohydrate, which is commercially available as Miramistin[®], exhibit high antibacterial and fungicidal activity [22].

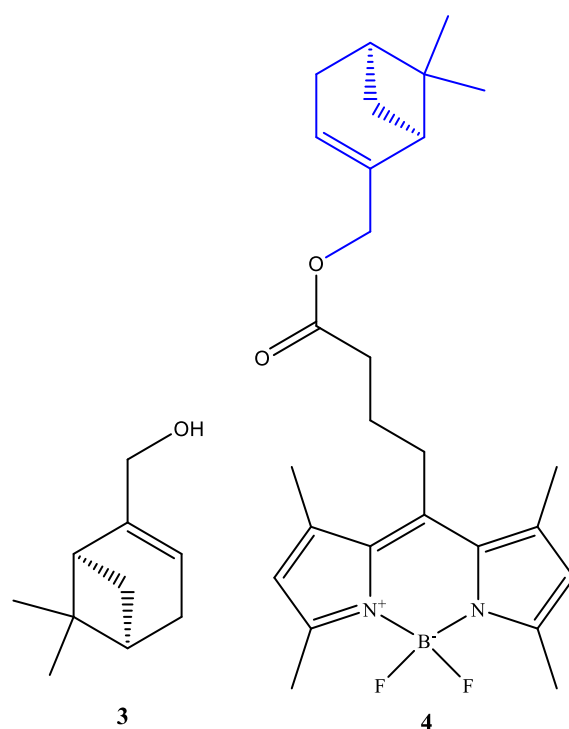


Figure 2. Structural representation of (+)-myrtenol **3** and BODIPY conjugate **4**.

The present paper aims to synthesize BODIPYs **10** and **11** and evaluate their luminescent properties, stability in aqueous and buffer media and affinity to various cells, to discover how the introduction of a charged quaternary ammonium fragments will affect the properties of compounds **10**, **11** compared to neutral BODIPY **1**, **2**, and **4** molecules offered as tools for biological object visualization.

2. Results and Discussion

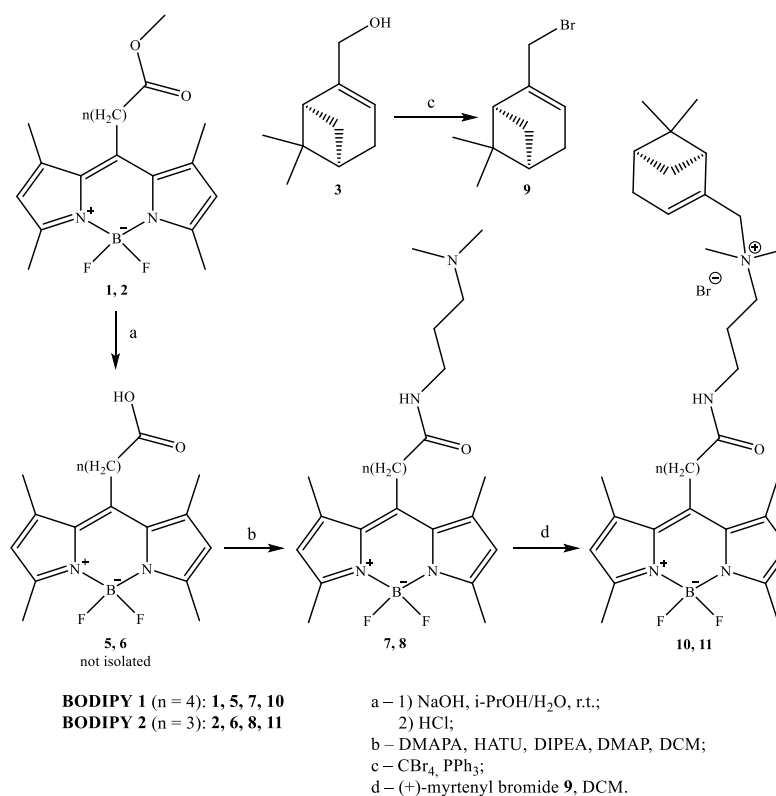
2.1. Synthesis

BODIPY amides **7**, **8** were generated by the alkaline hydrolysis of compounds **1**, **2** with alkali in aqueous isopropanol, followed by the reaction of the resulting acids **5**, **6** with dimethylaminopropylamine (DMAPA), hexafluorophosphate azabenzotriazole tetramethyl uronium (HATU), *N,N*-diisopropylethylamine (DIPEA) and 4-dimethylaminopyridine (DMAP) in dichloromethane (DCM) (Scheme 1). Furthermore, an excess of myrtenyl bromide **9** was added to BODIPY amides **7** or **8** in DCM at room temperature. After evaporation under low pressure, chromatography was performed to isolate target compounds **10** and **11**.

2.2. Spectral Properties

The spectral properties of BODIPY conjugates **10** and **11** were studied in 1-octanol, ethanol, *N,N*-dimethylformamide, dimethylsulfoxide and pure water. Boron(III) dipyrromethenates **1**, **2** and the myrtenol containing BODIPY conjugate **4** served as references. Quantitative spectral characteristics of the studied compounds are shown in Tables 1 and 2.

Regardless of the *meso*-substituent modification features, compounds **10**, **11** had a two-band electronic absorption spectrum typical of BODIPY dyes **1**, **2**, **4** (Table 1). The most intense long wavelength $S_0 \rightarrow S_1$ band were in the range of 495–500 nm, and the shoulder on its left slope appeared at 464–470 nm. In the shorter wavelength region 356–362 nm, a low-intensity broadened $S_0 \rightarrow S_2$ band occurred. The extinction coefficients (ϵ) of the intense $S_0 \rightarrow S_1$ band of compounds **10**, **11** were in the range from ~54,000 to ~60,000 $\text{l}\cdot\text{mol}^{-1}\cdot\text{cm}^{-1}$ (Table 1).

Scheme 1. Synthesis of compounds **10**, **11**.Table 1. Characteristics of electronic absorption spectra of compounds **1**, **2**, **4**, **10**, and **11** in various solvents.

Solvent	Compound				
	1 [23]	2 [23]	4 [23]	10	11
1-OctOH	502 (61,467) 358–364	499 (72,443) 357–364	501 (56,234) 357–364	500 (60,583) 358–364	499 (59,302) 360–365
EtOH	498 (60,491) 358–360	497 (72,444) 356–361	498 (45,708) 355–361	499 (57,420) 357–362	498 (58,379) 356–362
DMF	497 (61,659) 358–362	497 (76,709) 357–363	499 (48,669) 359–369	498 (56,846) 356–361	498 (55,615) 358–363
DMSO	498 (56,469) 359–362	497 (66,069) 356–363	499 (47,657) 355–360	500 (60,108) 357–360	498 (54,866) 357–361
Water	–	–	–	497 (56,853) 358–360	495 (54,748) 357–362

Notes: λ_{\max}^{abs} —maximum absorption bands ($S_0 \rightarrow S_1$, $S_0 \rightarrow S_2$), nm; ϵ —molar extinction coefficient, $l \cdot mol^{-1} \cdot cm^{-1}$.

Table 2. The luminescent characteristics of compounds **1**, **2**, **4**, **10**, and **11** in various solvents.

Solvent	1 [23]			2 [23]			4 [23]			10			11		
	λ_{ex}^{fl} (λ_{ex} 470) nm	$\Delta\nu_{St}$ cm^{-1}	φ	λ_{ex}^{fl} (λ_{ex} 470) nm	$\Delta\nu_{St}$ cm^{-1}	φ	λ_{ex}^{fl} (λ_{ex} 470) nm	$\Delta\nu_{St}$ cm^{-1}	φ	λ_{ex}^{fl} (λ_{ex} 480) nm	$\Delta\nu_{St}$ cm^{-1}	φ	λ_{ex}^{fl} (λ_{ex} 480) nm	$\Delta\nu_{St}$ cm^{-1}	φ
1-OctOH	516	540	0.96	515	623	0.98	516	580	0.95	511	431	0.70	511	471	0.66
EtOH	513	587	0.89	511	551	0.87	512	549	0.85	511	471	0.75	510	473	0.70
DMF	515	703	0.79	512	590	0.85	515	622	0.82	511	511	0.74	510	473	0.69
DMSO	515	662	0.74	512	590	0.78	515	622	0.78	511	511	0.74	510	473	0.72
Water	–	–	–	–	–	–	–	–	–	510	513	0.72	509	556	0.67

Notes: λ_{ex} , λ_{max}^{fl} —excitation and emission maxima, respectively, nm; $\Delta\nu_{St}$ —Stokes shift, cm^{-1} ; φ —fluorescence quantum yield.

Figure 3 shows typical absorption spectra of conjugate **10** in various solvents. Conjugates **10** and **11** and their corresponding BODIPY esters **1**, **2**, **4** intensely fluoresced at 509–516 nm, depending on the solvent nature (Table 2). The shape of the fluorophores **10** and **11** fluorescence band mirrors the intense $S_0 \rightarrow S_1$ absorption band with the Stokes shift $\Delta\nu_{St} = 431\text{--}556\text{ cm}^{-1}$ (Table 2, Figure 3). It should be noted that the introduction of both ester residues (compounds **1**, **2**, **4**) and substituents carrying a charged quaternary ammonium fragment (compounds **10**, **11**) into the *meso*-position of the BODIPY core caused a hypsochromic shift (by $\sim 14\text{--}18\text{ nm}$) of the maximum of the intense absorption band and a significant increase in the Stokes shift (up to $\sim 1.4\text{--}2.2$ fold) compared to *meso*-unsubstituted tetramethyl-BODIPY, for which $\Delta\nu_{St}$ does not exceed $271\text{--}461\text{ cm}^{-1}$ [24]. The observed effect can be caused by the BODIPY chromophore system depolarization because of the total electronic effects of the considered *meso*-substituents and a slight distortion of the chromophore aromatic system plane [23].

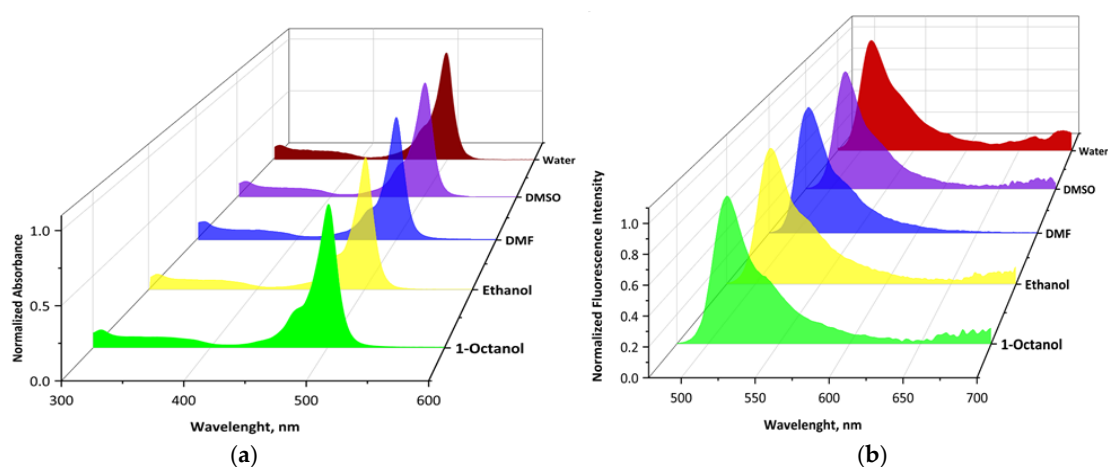


Figure 3. The normalized absorption (a) and fluorescence (b) spectra of conjugate **10** in different solvents.

Importantly, in contrast to hydrophobic BODIPYs [23–26], including dyes **1**, **2**, and **4**, the presence of charged quaternary ammonium fragments in the *meso*-substituent ensured the solubility of conjugates **10** and **11** to $\sim 10^{-5}\text{ mol}\cdot\text{l}^{-1}$ in water and buffer systems such as tetraoxalate buffer (pH 1.65), phosphate buffer (pH 7.21), and tetraborate buffer (pH 9.18). The luminophores were found to be stable under these environmental conditions (Tables 2 and 3 and Figure 4) and the intensity of their absorption (a) and fluorescence (b) band spectra almost did not change during 24 h in both acidic and alkaline media (Figure 4), indicating conjugates **10** and **11** as promising for various biomedical applications.

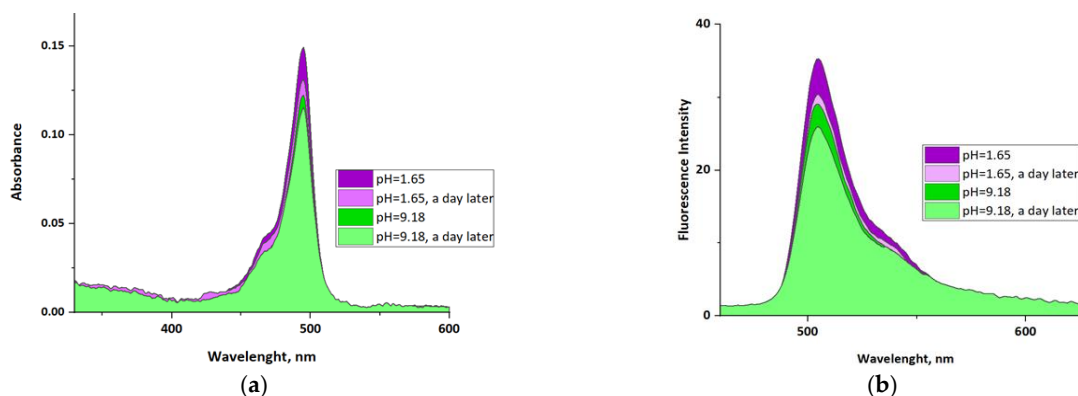


Figure 4. The absorption (a) and fluorescence ($\lambda_{exc} = 480\text{ nm}$) (b) spectra of conjugate **11** ($c \sim 10^{-6}\text{ mol}\cdot\text{L}^{-1}$) in time at different pH values.

Table 3. The fluorescence quantum yields of dyes **10** and **11** in different buffer systems.

Compound	Potassium Tetraoxalate Buffer, pH 1.65	Buffer Solution	Sodium Borate Buffer
		Phosphate Buffer, pH 7.21 φ	Buffer pH 9.18
10	0.41	0.46	0.46
11	0.46	0.49	0.47

The obtained data (Table 2) fit well with literature data [23] and allow the assumption that the introduction of bulky substituents into the *meso*-position has a marked effect on the fluorescence efficiency of the BODIPY conjugates **10** and **11**. In comparison with BODIPY **1**, **2**, and **4**, for dyes **10** and **11**, a significant decrease (up to ~30%) of the fluorescence quantum yield (φ) is apparently driven by a nonradiative energy loss, size increase, conformational rearrangements, and solvation dipole–dipole interactions of the *meso*-substituent (Table 2). Therefore, for all compounds, the spectral characteristics of fluorophores are almost independent of the solvent nature compared to, for example, phenylmethylene pyridineacetonitrile derivatives [23]. The absorption peak wavelength was barely shifted (by 1–4 nm) in the different solvents, indicating that the ground state charge transfer was hardly affected by the solvent polarity. A slight drop of fluorescence quantum yield of BODIPY **1**, **2**, and **4** by ~20% was observed upon transfer to more polar media due to the increased solvation of dipole–dipole interactions. On the other hand, for **10** and **11**, in both organic (nonpolar or polar) solvents and water, the values of φ almost did not change, while it decreased 1.3–1.8-fold in buffers (Table 3) because of the ion-dipole interactions with buffer components.

The lipophilicity of conjugates **10** and **11** was assessed using the distribution coefficient values of luminophores $\log P$ in the two-phase model system 1-octanol–water by the “shake flask” approach at 298.15 K, assuming the two-phase system to be a model cell membrane surrounded by the aqueous medium. A comparative analysis of the obtained and the literature data [23] showed that the partition coefficients increase in the sequence of dyes: **11** (0.14); **10** (0.16); **2** (1.68); **1** (1.83); **4** (1.87). The introduction of a charged quaternary ammonium residue into the *meso*-position of conjugates **10** and **11** led to a significant increase (almost ~9.3–13.4 fold) in the luminophor’s affinity to hydrophilic media compared to *meso*-substituted BODIPY esters **1**, **2**, and **4**, probably due to an increase in the hydrophilic solvation interaction efficiency.

2.3. Microscopy

Differential fluorescent staining is a common and widely used tool for both the quantitative and qualitative assessment of pro- and eukaryotic cell sub-population fractions and cellular organelles by using microscopy. Therefore, the development of new dyes with selectivity to given cells or their organelles, i.e., their membranes, cores, mitochondria, etc. is challenging. For fluorophore **2** and its conjugate with terpenoids and quaternary ammonium fragments, its ability to stain bacterial cells and penetrate the matrices of bacterial biofilms was assessed with confocal laser scanning microscopy. *S. aureus*, *P. aeruginosa* and *K. pneumoniae*, three of six most dangerous nosocomial pathogens called ESKAPE and which lead to development of biofilm-associated infections, were chosen as test objects. Mature 48 h biofilms of these bacteria were washed and loaded with PBS containing compounds at a final concentration of 10 $\mu\text{g}/\text{mL}$, incubated for 10 min at room temperature, and CLSM was performed. Additionally, instead of a bright-field view, cells were visualized by staining with the fluorescent dye DAPI.

The pure fluorophore **2** was able to stain the cells of all bacteria, including those embedded into the microbial biofilm matrix, and provided a high level of fluorescence (Figure 5A–C). In this case, the maximal signal was observed for *S. aureus* (3000 photons), while for Gram-negative *P. aeruginosa* and *K. pneumoniae*, the fluorescence intensity was

two-fold less (~1500 photons). The fusion of a myrtenol molecule to **2** drastically reduced the staining efficiency. Thus, while the observed fluorescence intensity of stained *S. aureus* and *P. aeruginosa* cells decreased 5-fold (compare Figure 5A,E, and Figure 5C,F), almost no staining of *K. pneumoniae* was observed (Figure 5E), also confirmed by the predominantly blue color of the cells in the overlaid image (Figure 6E). In turn, the introduction of an additional quaternary ammonium group into **4** facilitated the interaction of **11** with cells, since only a 1.5–2-fold decrease in fluorescence was observed compared to the pure fluorophore **2** (Figure 5G–I). Notably, **11** was almost completely localized in the membrane/cell wall of *S. aureus* (Figure 5G) and *K. pneumoniae* (Figure 5H), while *P. aeruginosa* cells were completely stained (Figure 5I).

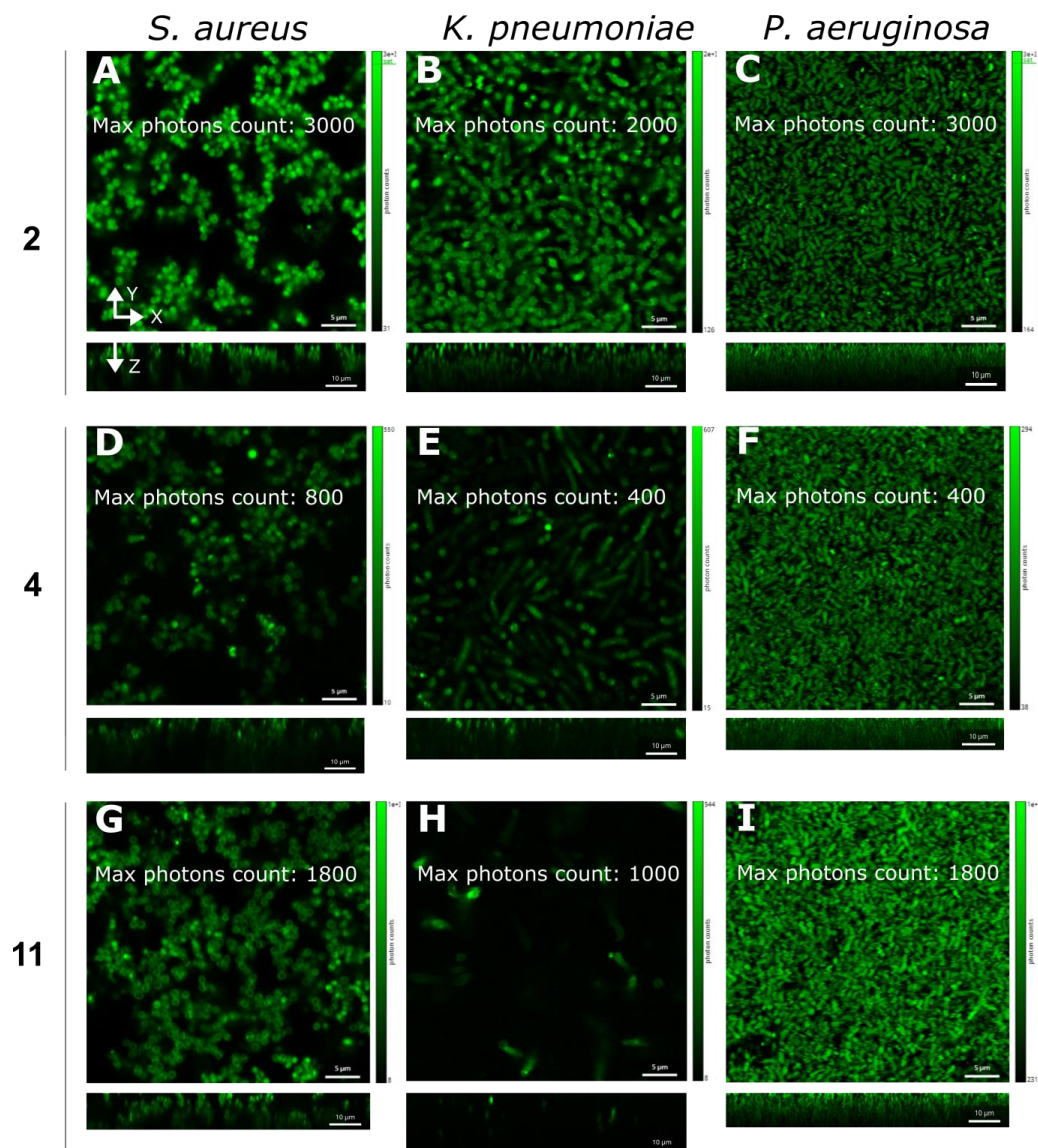


Figure 5. The penetration of compounds into bacterial cells. Solely fluorophore (**2**, A–C), fluorophore fused with myrtenol (**4**, D–F) and fluorophore fused with myrtenol via quaternary ammonium fragments (**11**, G–I) were added to preformed and PBS-washed 48 h old biofilms of *S. aureus* (A,D,G), *K. pneumoniae* (B,E,H) and *P. aeruginosa* (C,F,I) until final concentrations of 10 $\mu\text{g}/\text{mL}$. After 10 min incubation, cells were analyzed by confocal laser scanning microscopy with excitation/emission at 490/525 nm. Bars correspond to 5 μm in plain view and to 10 μm in Z-stacks. To comparatively evaluate the fluorescence intensity, the maximal photon counts (shown on the right as heat map legend) were normalized by compound molecular weights.

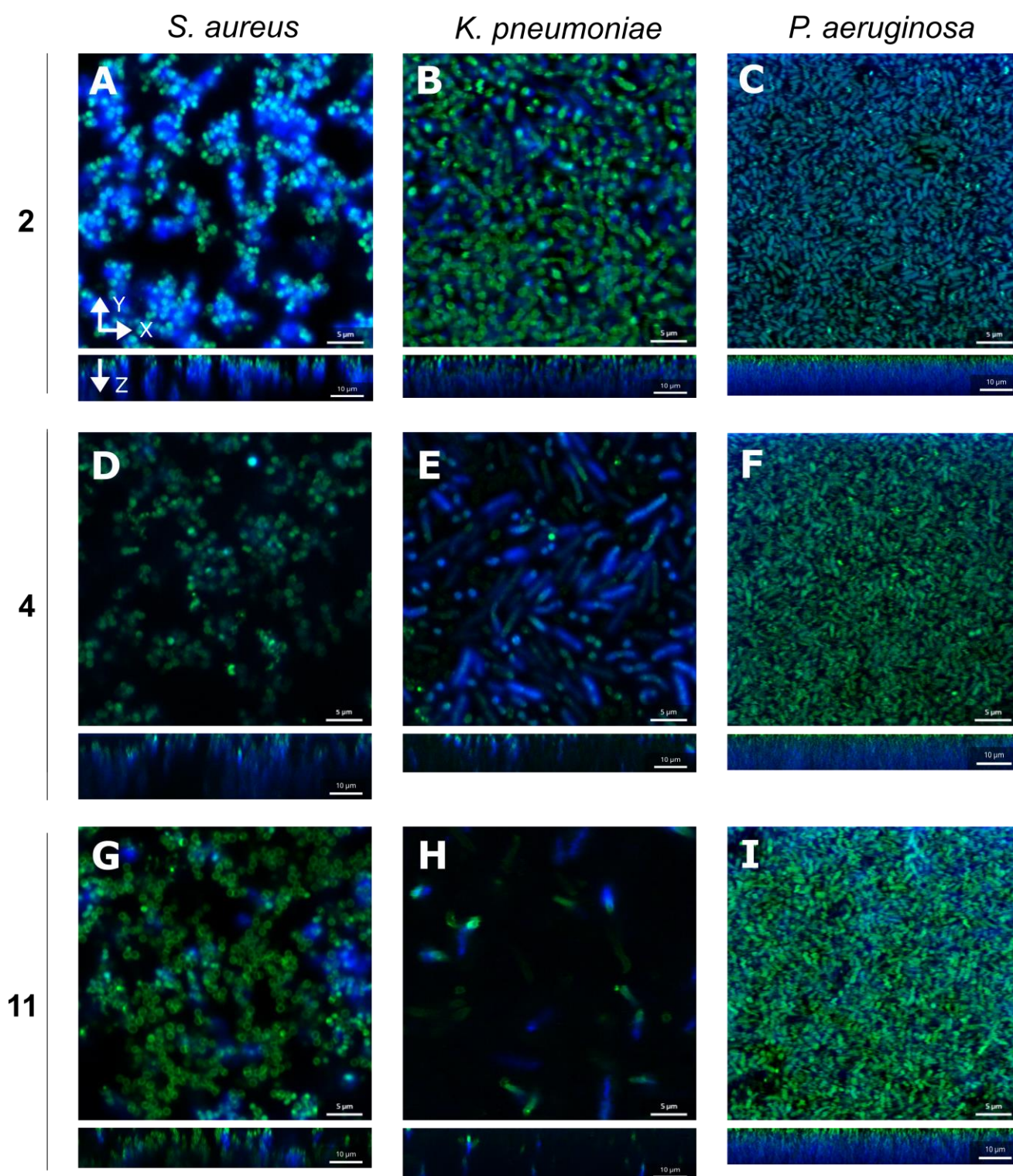


Figure 6. The penetration of compounds into bacterial cells. Solely fluorophore (2, A–C), fluorophore fused with myrtenol (4, D–F) and fluorophore fused with myrtenol via quaternary ammonium fragments (11, G–I) were added to preformed and PBS-washed 48 h old biofilms of *S. aureus* (A,D,G), *K. pneumoniae* (B,E,H) and *P. aeruginosa* (C,F,I) until final concentrations of 10 $\mu\text{g}/\text{mL}$. DAPI was added until a final concentration of 5 $\mu\text{g}/\text{mL}$. After 10 min incubation, images were captured by confocal laser scanning microscope with excitation/emission at 359/457 and 490/525 nm and overlaid. Bars correspond to 5 μm in plain view and to 10 μm in Z-stacks.

In marked contrast to bacteria, **2** was unable to penetrate into *F.solani* filaments (see Figure 7A,C), while the fusion of BODIPY with either myrtenol or myrtenol and a quaternary ammonium moiety facilitated the penetration of the dye into a fungal cell (see Figure 7D,G). Of note, the **4** and **11** seem to bind with organelles, probably mitochondria, since the treated filaments gave a grainy pattern on images.

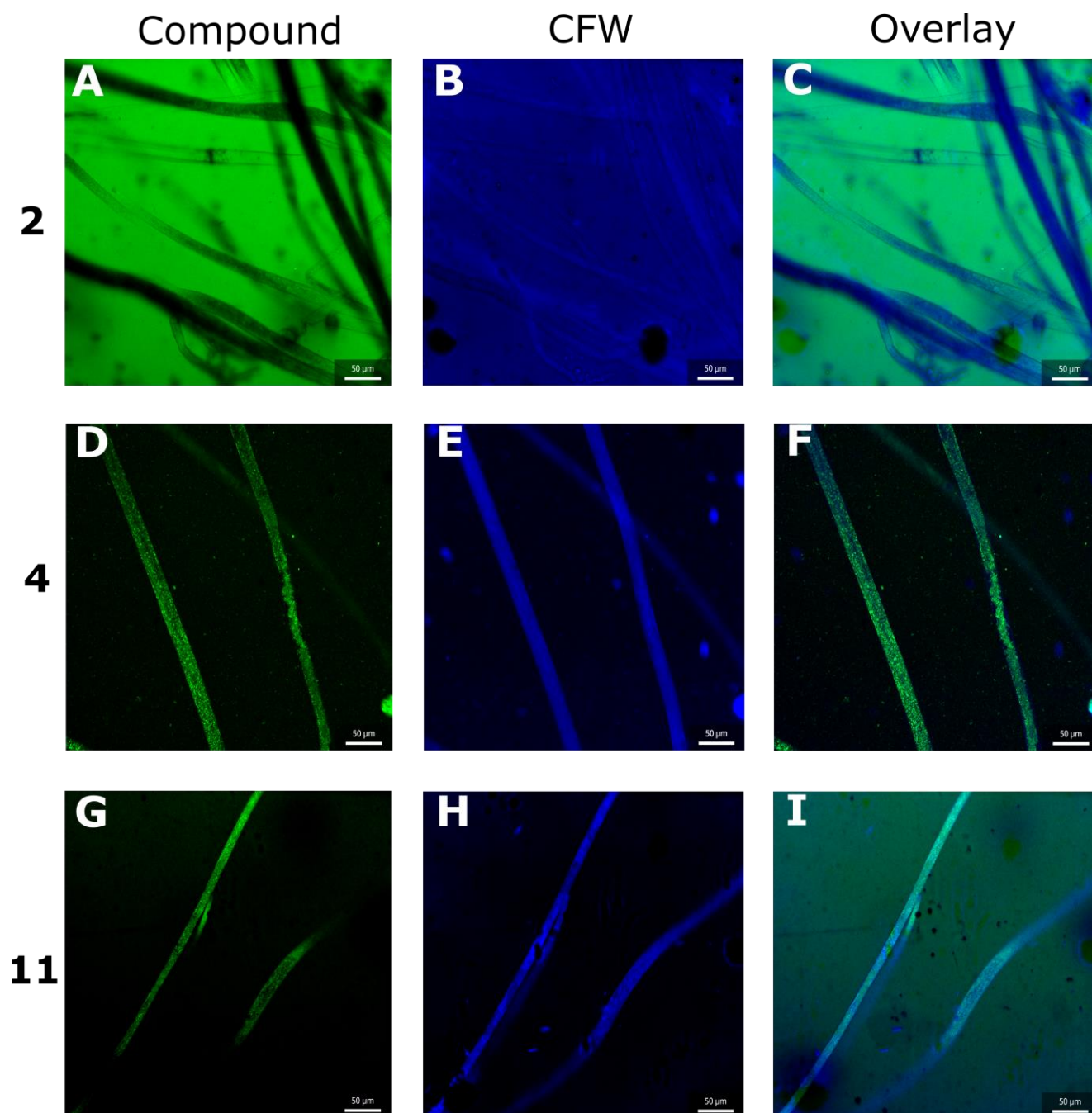


Figure 7. The penetration of compounds into filamentous fungi (*Fusarium solani*). The solely fluorophore (**2**, A–C), fluorophore fused with myrtenol (**4**, D–F) and fluorophore fused with myrtenol via quaternary ammonium fragments (**11**, G–I) were added to a *F. solani* filament suspension until the final concentrations of 10 µg/mL. Calcofluor (CFW) white was added until a final concentration of 5 µg/mL. After 10 min, incubation images were captured by confocal laser scanning microscope with excitation/emission at 359/457 and 490/525 nm and overlayed. Bars correspond to 50 µm.

3. Materials and Methods

3.1. General

Isopropanol, toluene, and dichloromethane were reagent grade and used without purification. Dimethylaminopropylamine, hexafluorophosphate azabenzotriazole tetramethyl uronium, *N,N*-diisopropylethylamine, 4-dimethylaminopyridine, tetrabromomethane and triphenylphosphine were purchased from Sigma-Aldrich (St. Louis, MO, USA). (+)-Myrtenol **3** and (+)-myrtenyl bromide **9** were prepared by a known procedure [27]. Reaction products were purified by flash chromatography on a PuriFlash Column, 15 μ C18 HP, 6g (eluent gradient water—methanol).

NMR spectra were recorded on a Bruker AVANCE-II-500 spectrometer with operating frequencies of 500 MHz (for ^1H) and 125 MHz (for ^{13}C) in CDCl_3 solvent using standard Bruker pulse programs. The numbering of atoms in the description of the NMR spectra differs from the numbering in the names of compounds. The spectra are shown in Supplementary Materials (Figures S1–S4).

HRMS mass spectra were obtained on a quadrupole time-of-flight (*t*, UHR-TOF) Bruker Daltonik GmbH, (Germany, Bremen), maXis impact mass spectrometer using ion Booster source (nebulizer gas nitrogen, a positive ionization polarity, capillary voltage 4000 V). Recording of the spectra was performed in “TOF MS” mode with a collision energy 10 eV, transfer time 110 μs and with resolution of more than 30,000 full-width half-maximum. Samples with the analyte concentration 5 $\mu\text{mol/L}$ were prepared by dissolving the test compounds in a mixture of methanol (HPLC-UV Grade, LabScan) and water (LC-MS Grade, Panreac) in a 1:1 ratio.

3.2. General Procedure for Synthesis of BODIPYs **7**, **8**

BODIPY **1** (0.057 mmol) or **2** (0.059 mmol) in isopropanol (5 mL) were stirred with 0.1 N NaOH (1 mL) at room temperature for 1 h and evaporated. Then, toluene (10 mL) and diluted aqueous HCl were added to the mixtures with intensive stirring for neutralization. The organic phases were separated and evaporated under low pressure. To round bottom flasks containing not-isolated **5** or **6** in DCM (15 mL) HATU (0.060 mmol), DIPEA (0.115 mmol), DMAP (0.060 mmol) and equimolar amounts of DMAPA were added. Reaction mixtures were stirred for 1 h at room temperature. After evaporation under low pressure, reaction products were purified to afford amides **7** (orange crystals, yield 70%) and **8** (orange crystals, yield 74%).

3.3. General Procedure for Synthesis of BODIPY Conjugates **10**, **11**

To BODIPY amides **7** (0.039 mmol) or **8** (0.044 mmol) in round bottom flasks, DCM (10 mL) and an excess of myrtenyl bromide **9** (0.13 mmol) were added and stirred for 40 min at room temperature. After evaporation under low pressure, chromatography was performed to provide target compounds **10** and **11**.

BF_2 -*meso*-(4-pentanamido-*N*-(((1*S*,5*R*)-6,6-dimethylbicyclo[3.1.1]hept-2-en-2-yl)methyl)-*N,N*-dimethylpropan-1-aminium)-3,3',5,5'-tetramethyl-2,2'-dipyrrromethene bromide (**10**). Viscous orange oil. Yield: 70%. $[\alpha]_D^{23} = +8.0^\circ$ (c 0.16; MeOH).

NMR ^1H (CDCl_3) δ , ppm: 0.74 (s, 6H, CH_3 -1,2), 1.06 (s, 6H, CH_3 -21,22), 1.24 (s, 2H, CH_2 -17), 1.56 (m, 4H, CH_2 -5,16), 1.77 (m, 2H, CH_2 -6), 1.91 (s, 2H, CH_2 -5'), 2.00 (s, 5H, CH -4, CH_2 -15), 2.10 (s, 2H, CH_2 -6'), 2.14 (m, 2H, CH_2 -18), 2.34 (s, 1H, CH -3), 2.37 (s, 6H, CH_3 -19,24), 2.86 (s, 6H, CH_3 -9,10), 2.90 (m, 2H, CH_2 -11), 3.26 (s, 1H, CH -20,23), 3.62 (m, 4H, CH_2 -8,12), 3.74 (q, 2H, CH_2 -13, $J = 104.3; 11.9$), 5.98 (s, 1H, CH -7), 8.19 (s, 1H, NH -14).

NMR ^{13}C $\{^1\text{H}\}$ (CDCl_3) δ , ppm: 14.6 (CH_3 -21,24), 16.7 (CH_3 -22), 21.4 (CH_3 -19), 23.0 (CH_2 -12), 26.1 (CH_3 -1,2), 26.3 (CH_2 -17), 28.5 (CH_2 -16), 31.6 (CH_2 -18), 32.0 (CH_2 -6), 32.3 (CH_2 -5), 35.8 (CH_2 -15), 36.1 (C -25), 38.2 (CH_2 -13), 39.8 (CH -4), 47.2 (CH -3), 49.9 (CH_3 -10), 50.1 (CH_3 -9), 63.4 (CH_2 -11), 70.1 (CH_2 -8), 121.9 (CH -20, C -32), 125.5 (C -31), 128.4 (CH -7), 129.2 (C -26), 131.5 (CH -23), 135.9 (C -27), 136.8 (C -29), 141.1 (C -33), 146.6 (C -28), 153.9 (C -30), 173.9 (CO -14).

HRMS: m/z $[\text{M}]^+$ calcul. for $\text{C}_{33}\text{H}_{50}\text{BF}_2\text{N}_4\text{O}^+$: 567.60; found: 567.4046.

BF₂-*meso*-(4-butanamido-*N*-(((1*S*,5*R*)-6,6-dimethylbicyclo[3.1.1]hept-2-en-2-yl)methyl)-*N,N*-dimethylpropan-1-aminium)-3,3',5,5'-tetramethyl-2,2'-dipyrrromethene bromide (**11**). Viscous orange oil. Yield: 61%. $[\alpha]^{23}_D = +35.5^\circ$ (c 0.14; MeOH).

NMR ¹H (CDCl₃) δ, ppm: 0.85 (s, 6H, CH₃-1,2), 1.17 (s, 6H, CH₃-21,22), 1.33 (s, 2H, CH₂-17), 1.43 (m, 2H, CH₂-16), 1.96 (m, 2H, CH₂-5), 2.09 (s, 2H, CH₂-6), 2.20 (s, 2H, CH₂-5'), 2.26 (s, 1H, CH-4), 2.43 (s, 2H, CH₂-6'), 2.47 (s, 6H, CH₃-19,24), 2.57 (m, 2H, CH₂-15), 2.63 (s, 1H, CH-3), 3.05 (m, 2H, CH₂-11), 3.09 (s, 6H, CH₃-9,10), 3.39 (s, 2H, CH-20,23), 3.79 (q, 2H, CH₂-12, J = 104.3;11.9), 3.84 (m, 2H, CH₂-8), 3.89 (q, 2H, CH₂-13, J = 104.3;11.9), 6.10 (s, 1H, CH-7), 8.62 (s, 1H, NH-14).

NMR ¹³C {¹H} (CDCl₃) δ, ppm: 14.4 (CH₃-21,24), 16.6 (CH₃-22), 21.3 (CH₂-12, CH₃-19), 22.7 (CH₃-1,2), 25.9 (CH₂-17), 27.9 (CH₂-16), 31.9 (CH₂-6), 32.2 (CH₂-5), 36.2 (CH₂-15), 38.1 (C-25), 39.7 (CH₂-13), 45.9 (CH-4), 47.2 (CH-3), 50.0 (CH₃-9,10), 63.2 (CH₂-11), 70.2 (CH₂-8), 121.6 (CH-20, C-32), 128.2 (C-31), 129.8 (CH-7), 130.9 (C-26), 131.5 (CH-23), 135.8 (C-27), 136.7 (C-29), 141.0 (C-33), 146.0 (C-28), 153.8 (C-30), 173.3 (CO-14).

HRMS: *m/z* [M]⁺ calcul. for C₃₂H₄₈BF₂N₄O⁺: 553.57; found: 553.3889.

3.4. Instruments and Methods

Fluorescence quantum yields (φ) were determined in accordance with the equation [28] according to the equation:

$$\varphi = \varphi^{st} \cdot \frac{S^x}{S^{st}} \cdot \frac{A^{st}}{A^x} \cdot \left(\frac{n^x}{n^{st}}\right)^2.$$

where φ and φ^{st} are the quantum yields of the sample and standard, S^x and S^{st} are the area under the emission spectrum of the sample and the standard, A^x and A^{st} are the optical density in the absorption spectrum of the sample and the standard at the excitation wavelength, and n is the refractive index of the medium. As a standard for determining the fluorescence quantum yield, we used ethanol solution of Rhodamine 6G with a known [29] value of the quantum yield ($\varphi = 0.94$) in ethanol.

The compound distribution coefficient (P) was obtained by measuring the dye concentrations in the water–1-octanol phases. BODIPYs were dissolved in 1-octanol (4.2–7.1 μM). The solutions were mixed with water (1 to 1). The mixture was stirred for 8 h at 25 °C. After equilibration, the systems were separated. The logP was calculated by Equation (1): $\log P = \log([\text{dye}]_{1\text{-octanol}}/[\text{dye}]_{\text{water}})$.

3.5. Strains and Growth Conditions

Staphylococcus aureus subsp. *aureus* ATCC[®] 29213[™], *Pseudomonas aeruginosa* ATCC[®] 27853[™] and *Klebsiella pneumoniae* subsp. *pneumoniae* ATCC[®] 13883[™] were used in the study. Bacteria were stored as a 50% glycerol stock at –80 °C and maintained in the LB medium. Biofilms were grown for 48 h in the BM broth (glucose 5 g, peptone 7 g, MgSO₄ × 7H₂O 2.0 g and CaCl₂ × 2H₂O 0.05 g in 1.0 L tap water) [30–32] at 37 °C under static conditions in imaging cover slips (Eppendorf). Furthermore, a clinical isolate of *Fusarium solani* F-417 isolated from the skin was obtained from the collection of the Kazan Institute of Microbiology and Epidemiology (Kazan, Russia). A 5-day-old culture of fungi grown on Sabouraud's solid nutrient medium was suspended in RPMI (Roswell Park Memorial Institute) broth and seeded with fungi until 1 × 10⁵ cells/mL.

3.6. Microscopy

The penetration of compounds into mature bacterial biofilms and fungal cells was assessed with confocal laser scanning microscopy. For this, mature 48 h biofilms on cell imaging cover slips (Eppendorf) were stained with DAPI (5 μg/mL) and compounds (10 μg/mL). Fungal cells were stained with compounds (10 μg/mL) for 10 min. To assess the localization of the tested fluorophores in fungal cells, a fluorescent blue dye, calcofluor white (CFW), was used. Compound localization was analyzed by an Olympus IX83 inverted microscope supplemented with a STEDYCON ultrawide extension platform.

4. Conclusions

Thus, we demonstrated the effect of various *meso*-substituents in BODIPY molecules (*BF*₂-*meso*-(4-butan/pentanamido-*N*-(((1*S*,5*R*)-6,6-dimethylbicyclo[3.1.1]hept-2-en-2-yl)methyl)-*N,N*-dimethylpropan-1-aminium)-3,3',5,5'-tetramethyl-2,2'-dipyrrromethene bromides) on their properties. Thus, the fusion of myrtenol, a monocyclic terpene, to the BODIPY fluorophore in the *meso*-substituent facilitated its penetration into filamentous fungi *F. solani*, while impairing the binding of the latter with *S. aureus*, *K. pneumoniae* and *P. aeruginosa*. The additional quaternary ammonium group between myrtenol and the fluorophore moieties restored the bacterial cells staining, but did not affect staining of the fungi. Both the BODYPI fusions with solely myrtenol, and the myrtenol bound with quaternary ammonium, did not bind with the fungal cell wall and gave grainy images, apparently because of binding with organelles, probably mitochondria. The BODIPY fused to myrtenol via the quaternary ammonium group exhibited high fluorescence efficiency in media of various natures and stabilities over a wide pH range, demonstrating the practical potential of the synthesized BODIPY conjugates as fluorescent markers for biomedical applications.

Supplementary Materials: The following supporting information can be downloaded at: <https://www.mdpi.com/article/10.3390/inorganics11060241/s1>, Figure S1: ¹H NMR spectrum of *BF*₂-*meso*-(4-pentanamido-*N*-(((1*S*,5*R*)-6,6-dimethylbicyclo[3.1.1]hept-2-en-2-yl)methyl)-*N,N*-dimethylpropan-1-aminium)-3,3',5,5'-tetramethyl-2,2'-dipyrrromethene bromide (**10**) in CDCl₃, Figure S2: ¹³C NMR spectrum of *BF*₂-*meso*-(4-pentanamido-*N*-(((1*S*,5*R*)-6,6-dimethylbicyclo[3.1.1]hept-2-en-2-yl)methyl)-*N,N*-dimethylpropan-1-aminium)-3,3',5,5'-tetramethyl-2,2'-dipyrrromethene bromide (**10**) in CDCl₃, Figure S3: ¹H NMR spectrum of *BF*₂-*meso*-(4-butanamido-*N*-(((1*S*,5*R*)-6,6-dimethylbicyclo[3.1.1]hept-2-en-2-yl)methyl)-*N,N*-dimethylpropan-1-aminium)-3,3',5,5'-tetramethyl-2,2'-dipyrrromethene bromide (**11**) in CDCl₃, Figure S4: ¹³C NMR spectrum of *BF*₂-*meso*-(4-butanamido-*N*-(((1*S*,5*R*)-6,6-dimethylbicyclo[3.1.1]hept-2-en-2-yl)methyl)-*N,N*-dimethylpropan-1-aminium)-3,3',5,5'-tetramethyl-2,2'-dipyrrromethene bromide (**11**) in CDCl₃.

Author Contributions: Conceptualization, L.E.N. and R.S.P.; formal analysis, E.V.A., M.B.B., I.R.G., S.A.L., L.L.F., O.V.O., I.Z.R. and E.Y.T.; funding acquisition, G.B.G., L.E.N. and A.R.K.; investigation, G.B.G., E.V.A., M.B.B., I.R.G., S.A.L., L.L.F., I.Z.R. and E.Y.T.; methodology, G.B.G., E.V.A., M.B.B., L.E.N., I.R.G., R.S.P., S.A.L., L.L.F., I.Z.R. and E.Y.T.; project administration, G.B.G., L.E.N. and A.R.K.; supervision, R.S.P. and V.V.K.; visualization, G.B.G., E.V.A., L.E.N., I.R.G., R.S.P., S.A.L., I.Z.R. and A.R.K.; writing—original draft, G.B.G., L.E.N., I.R.G., S.A.L., I.Z.R. and A.R.K.; writing—review and editing, G.B.G., L.E.N. and A.R.K. All authors have read and agreed to the published version of the manuscript.

Funding: This study was performed with financial support from the Russian Science Foundation (grant N 20-64-47014 for A.R.K. (<https://rscf.ru/en/project/20-64-47014/>, accessed on 15 April 2023)—microscopy and NMR, grant N 20-63-47026 for E.V.A. (<https://rscf.ru/en/project/20-63-47026/>, accessed on 15 April 2023)—the spectral investigations and pH-stability) and Kazan State Medical University (Project N 58-012-2022 for L.E.N.—synthetic procedures).

Data Availability Statement: Not applicable.

Acknowledgments: This work was performed in frames of the Strategic Academic Leadership Program (PRIORITY-2030) of Kazan Federal University.

Conflicts of Interest: The authors declare no conflict of interest.

References

1. Antina, E.; Bumagina, N.; Marfin, Y.; Guseva, G.; Nikitina, L.; Sbytov, D.; Telegin, F. BODIPY Conjugates as Functional Compounds for Medical Diagnostics and Treatment. *Molecules* **2022**, *27*, 1396. [[CrossRef](#)] [[PubMed](#)]
2. Fu, Y.; Finney, N.S. Small-molecule fluorescent probes and their design. *RSC Adv.* **2018**, *8*, 29051–29061. [[CrossRef](#)]
3. Yao, W.; Wang, J.; Zhong, A.; Wang, S.; Shao, Y. Transition-metal-free catalytic hydroboration reduction of amides to amines. *Org. Chem. Front.* **2020**, *7*, 3515–3520. [[CrossRef](#)]
4. Liu, H.; Zhang, X.-F.; Cheng, J.-Z.; Zhong, A.-G.; Wen, H.-R.; Liu, S.-Y. Novel Diketopyrrolopyrrole-Based π -Conjugated Molecules Synthesized via One-Pot Direct Arylation Reaction. *Molecules* **2019**, *24*, 1760. [[CrossRef](#)] [[PubMed](#)]

5. Sun, H.; Chen, S.; Zhong, A.; Sun, R.; Jin, J.; Yang, J.; Liu, D.; Niu, J.; Lu, S. Tuning Photophysical Properties via Positional Isomerization of the Pyridine Ring in Donor–Acceptor-Structured Aggregation-Induced Emission Luminogens Based on Phenylmethylene Pyridineacetonitrile Derivatives. *Molecules* **2023**, *28*, 3282. [[CrossRef](#)] [[PubMed](#)]
6. Li, C.; Chen, G.; Zhang, Y.; Wu, F.; Wang, Q. Advanced Fluorescence Imaging Technology in the Near-Infrared-II Window for Biomedical Applications. *J. Am. Chem. Soc.* **2020**, *142*, 14789–14804. [[CrossRef](#)] [[PubMed](#)]
7. Cheng, H.; Cao, X.; Zhang, S.; Zhang, K.; Cheng, Y.; Wang, J.; Zhao, J.; Zhou, L.; Liang, X.; Yoon, J. BODIPY as a Multifunctional Theranostic Reagent in Biomedicine: Selficine: Self; Cperties, and Applications. *Adv. Mater.* **2022**, *35*, e2207546. [[CrossRef](#)]
8. Guseva, G.B.; Antina, E.V.; Berezin, M.B.; Pavelyev, R.S.; Kayumov, A.R.; Sharafutdinov, I.S.; Lisovskaya, S.A.; Lodochnikova, O.A.; Islamov, D.R.; Usachev, K.S. Meso-substituted-BODIPY based fluorescent biomarker: Spectral characteristics, photostability and possibilities for practical application. *J. Photochem. Photobiol. A Chem.* **2020**, *401*, 112783. [[CrossRef](#)]
9. Guseva, G.; Antina, E.; Berezin, M.; Lisovskaya, S.; Pavelyev, R.; Kayumov, A.; Lodochnikova, O.; Islamov, D.; Usachev, K.; Boichuk, S.; et al. Spectroscopic and In Vitro Investigations of Boron(III) Complex with *Meso*-4-Methoxycarbonylpropylsubstituted Dipyrromethene for Fluorescence Bioimaging Applications. *Molecules* **2020**, *25*, 4541. [[CrossRef](#)]
10. Jantra, S.; Butta, P.; Jithavech, P.; Rojsitthisak, P.; Palaga, T.; Rashatasakhon, P.; Sukwattanasinitt, M.; Wacharasindhu, S. “Turn on” orange fluorescent probe based on styryl-BODIPY for detection of hypochlorite and its application in live cell imaging. *Dye. Pigment.* **2019**, *162*, 189–195. [[CrossRef](#)]
11. Solomonov, A.V.; Marfin, Y.; Romyantsev, E.V. Design and applications of dipyrin-based fluorescent dyes and related organic luminophores: From individual compounds to supramolecular self-assembled systems. *Dye. Pigment.* **2019**, *162*, 517–542. [[CrossRef](#)]
12. West, R.; Panagabko, C.; Atkinson, J. Synthesis and characterization of BODIPY- α -tocopherol: A fluorescent form of vitamin E. *J. Org. Chem.* **2010**, *75*, 2883–2892. [[CrossRef](#)] [[PubMed](#)]
13. Alekseeva, A.; Tretiakova, D.; Melnikova, D.; Molotkovsky, U.G.; Boldyrev, I. Novel fluorescent membrane probe 2, 3; 5, 6-bis (cyclohexyl)-BODIPY-labeled phosphatidylcholine. *Russ. J. Bioorganic Chem.* **2016**, *42*, 305–309. [[CrossRef](#)]
14. Guseva, G.B.; Antina, E.V.; Berezin, M.B.; Pavelyev, R.S.; Kayumov, A.R.; Ostolopovskaya, O.V.; Gilfanov, I.R.; Frolova, L.L.; Kutchin, A.V.; Akhverdiev, R.F.; et al. Design, Spectral Characteristics, and Possibilities for Practical Application of BODIPY FL-Labeled Monoterpenoid. *ACS Appl. Bio Mater.* **2021**, *4*, 6227–6235. [[CrossRef](#)] [[PubMed](#)]
15. Mockute, D.; Judzentiene, A. Variability of the essential oils composition of *Achillea millefolium* ssp. *millefolium* growing wild in Lithuania. *Biochem. Syst. Ecol.* **2003**, *31*, 1033–1045. [[CrossRef](#)]
16. Ngan, L.T.M.; Moon, J.-K.; Shibamoto, T.; Ahn, Y.-J. Growth-Inhibiting, Bactericidal, and Urease Inhibitory Effects of *Paeonia lactiflora* Root Constituents and Related Compounds on Antibiotic-Susceptible and -Resistant Strains of *Helicobacter pylori*. *J. Agric. Food Chem.* **2012**, *60*, 9062–9073. [[CrossRef](#)]
17. Silva, R.O.; Salvadori, M.S.; Sousa, F.B.M.; Santos, M.S.; Carvalho, N.S.; Sousa, D.P.; Gomes, B.S.; Oliveira, F.A.; Bar-bosa, A.L.R.; Freitas, R.M. Evaluation of the antihe antif the antiaantinoceptive effects of myrtenol, a plant a plantnmonoterpene alcohol, in mice. *Flavour Fragr. J.* **2014**, *29*, 184–192. [[CrossRef](#)]
18. Nikitina, L.E.; Startseva, V.A.; Dorofeeva, L.Y.; Artemova, N.P.; Kuznetsov, I.V.; Lisovskaya, S.A.; Glushko, N. Antifungal activity of bicyclic monoterpenoids and terpenesulfides. *Chem. Nat. Compd.* **2010**, *46*, 28–32. [[CrossRef](#)]
19. Nikitina, L.; Startseva, V.; Vakulenko, I.; Khismatulina, I.; Lisovskaya, S.; Glushko, N.; Fassakhov, R. Synthesis and anti-fungal activity of compounds of the pinane series. *Pharm. Chem. J.* **2009**, *43*, 251–254. [[CrossRef](#)]
20. Micucci, M.; Bolchi, C.; Budriesi, R.; Cevenini, M.; Maroni, L.; Capozza, S.; Chiarini, A.; Pallavicini, M.; Angeletti, A. Anti-hypertensive phytocomplexes of proven efficacy and well-established use: Mode of action and individual characterization of the active constituents. *Phytochemistry* **2020**, *170*, 112222. [[CrossRef](#)]
21. Mahmoud, R.Y.; Trizna, E.Y.; Sulaiman, R.K.; Pavelyev, R.S.; Gilfanov, I.R.; Lisovskaya, S.A.; Ostolopovskaya, O.V.; Frolova, L.L.; Kutchin, A.V.; Guseva, G.B.; et al. Increasing the Efficacy of Treatment of *Staphylococcus aureus*–*Candida albicans* Mixed Infections with Myrtenol. *Antibiotics* **2022**, *11*, 1743. [[CrossRef](#)] [[PubMed](#)]
22. Agafonova, M.N.; Kazakova, R.R.; Lubina, A.P.; Zeldi, M.I.; Nikitina, E.V.; Balakin, K.V.; Shtyrlin, Y.G. Antibacterial activity profile of miramistin in in vitro and in vivo models. *Microb. Pathog.* **2020**, *142*, 104072. [[CrossRef](#)]
23. Guseva, G.B.; Ksenofontov, A.A.; Bocharov, P.S.; Antina, E.V.; Nikitina, L.E. Effect of meso-substituent and solvent nature on spectral properties, pH-stability and affinity to blood transport proteins of BODIPY dyes. *J. Mol. Liq.* **2023**, *371*, 121078. [[CrossRef](#)]
24. Berezin, M.; Antina, E.; Guseva, G.; Kritskaya, A.Y.; Semeikin, A. Effect of meso-phenyl substitution on spectral properties, photo-and thermal stability of boron (III) and zinc (II) dipyrrometenates. *Inorg. Chem. Commun.* **2020**, *111*, 107611. [[CrossRef](#)]
25. Guo, B.; Peng, X.; Cui, A.; Wu, Y.; Tian, M.; Zhang, L.; Chen, X.; Gao, Y. Synthesis and spectral properties of new boron dipyrromethene dyes. *Dye. Pigment.* **2007**, *73*, 206–210. [[CrossRef](#)]
26. Nuraneeva, E.; Guseva, G.; Antina, E.; Kuznetsova, R.; Berezin, M.; V'yugin, A. Synthesis, spectral luminescent properties, and photostability of monoiodo-and dibromo-substituted BF₂-dipyrinates. *Russ. J. Gen. Chem.* **2016**, *86*, 840–847. [[CrossRef](#)]
27. Liu, H.-X.; Tan, H.-B.; He, M.-T.; Li, L.; Wang, Y.-H.; Long, C.-L. Isolation and synthesis of two hydroxychavicol heterodimers from *Piper nudibaccatum*. *Tetrahedron* **2015**, *71*, 2369–2375. [[CrossRef](#)]
28. Lakowicz, J.R. *Principles of Fluorescence Spectroscopy*; Springer: Berlin/Heidelberg, Germany, 2006.
29. Fischer, M.; Georges, J. Fluorescence quantum yield of rhodamine 6G in ethanol as a function of concentration using thermal lens spectrometry. *Chem. Phys. Lett.* **1996**, *260*, 115–118. [[CrossRef](#)]

30. Baidamshina, D.R.; Trizna, E.Y.; Holyavka, M.G.; Bogachev, M.I.; Artyukhov, V.G.; Akhatova, F.S.; Rozhina, E.V.; Fakhrullin, R.F.; Kayumov, A.R. Targeting microbial biofilms using Ficin, a nonspecific plant protease. *Sci. Rep.* **2017**, *7*, srep46068. [[CrossRef](#)]
31. Kayumov, A.R.; Nureeva, A.A.; Trizna, E.Y.; Gazizova, G.R.; Bogachev, M.I.; Shtyrlin, N.V.; Pugachev, M.V.; Sapozhnikov, S.V.; Shtyrlin, Y.G. New Derivatives of Pyridoxine Exhibit High Antibacterial Activity against Biofilm-Embedded *Staphylococcus* Cells. *BioMed Res. Int.* **2015**, *2015*, 890968. [[CrossRef](#)]
32. Kayumov, A.; Khakimullina, E.N.; Sharafutdinov, I.; Trizna, E.Y.; Latypova, L.Z.; Lien, H.T.; Margulis, A.B.; Bogachev, M.; Kurbangalieva, A.R. Inhibition of biofilm formation in *Bacillus subtilis* by new halogenated furanones. *J. Antibiot.* **2015**, *68*, 297–301. [[CrossRef](#)] [[PubMed](#)]

Disclaimer/Publisher's Note: The statements, opinions and data contained in all publications are solely those of the individual author(s) and contributor(s) and not of MDPI and/or the editor(s). MDPI and/or the editor(s) disclaim responsibility for any injury to people or property resulting from any ideas, methods, instructions or products referred to in the content.